ANALYTICAL MODELING OF DEVICE–CIRCUIT INTERACTIONS FOR THE POWER INSULATED GATE BIPOLAR TRANSISTOR (IGBT)*

ALLEN R. HEFNER, JR.
MEMBER, IEEE
Semiconductor Electronics Division
National Bureau of Standards
Gaithersburg, MD 20899

ABSTRACT–The device-circuit interactions of the power Insulated Gate Bipolar Transistor (IGBT) for a series resistor-inductor load, both with and without a snubber, are simulated. An analytical model for the transient operation of the IGBT, previously developed, is used in conjunction with the load circuit state equations for the simulations. The simulated results are compared with experimental results for all conditions. Devices with a variety of base lifetimes are studied. For the fastest devices studied (base lifetime = 0.3 μs), the voltage overshoot of the series resistor-inductor load circuit approaches the device voltage rating (500 V) for load inductances greater than 1 μH. For slower devices, though, the voltage overshoot is much less and a larger inductance can therefore be switched without a snubber circuit (e.g., 80 μH for a 7.1-μs device). In this study, the simulations are used to determine the conditions for which the different devices can be switched safely without a snubber protection circuit. Simulations are also used to determine the required values and ratings for protection circuit components when protection circuits are necessary.

I. INTRODUCTION

Recently, a new power device structure has been introduced which is designed to overcome the high on-state loss of the power MOSFET while maintaining the simple gate drive requirements of that device [1,2]. The devices are controlled at the input by a voltage, such as for a MOSFET, but the output current is characteristic of that of a bipolar transistor, hence the name Insulated Gate Bipolar Transistor (IGBT). A schematic of the structure of two of the several thousand cells of an n-channel IGBT is shown in Fig. 1.

The IGBT functions as a bipolar transistor that is supplied base current by a MOSFET [3]. This basic equivalent circuit of the IGBT is shown in Fig. 2 and the regions of each of these components are labeled on the right half of Fig. 1. The bipolar transistor of the IGBT consists of a low-doped, wide base, with the base virtual contact near the collector end of the base. This transistor has a low gain and is in the high-level injection condition for the practical current density range of the IGBT. To model the low-gain, high-level injection characteristics of the bipolar transistor of the IGBT, ambipolar transport must be used to describe the transport of electrons and holes in the base, and the quasi-static approximation cannot be used to describe the transient operation [4-7].

An analytical model has been developed [4,5] which accurately simulates the on-state current-voltage characteristics and the transient current and voltage waveforms of the IGBT for general loading conditions. In this paper, the analytical device model is used in conjunction with the load circuit state equations to simulate the current and voltage switching transient waveforms for a series resistor-inductor load with a snubber protection circuit added. For a 30-Ω load resistor, it is shown that a protection circuit is needed to prevent excessive voltage overshoot when the series load inductance is larger than 1 μH for a 0.3-μs device, 40 μH for a 2.4-μs device, and 80 μH for a 7.1-μs device. The model is then used to select the appropriate protection circuit components. The simulated current and voltage waveforms are compared with measurements for all of the conditions studied.

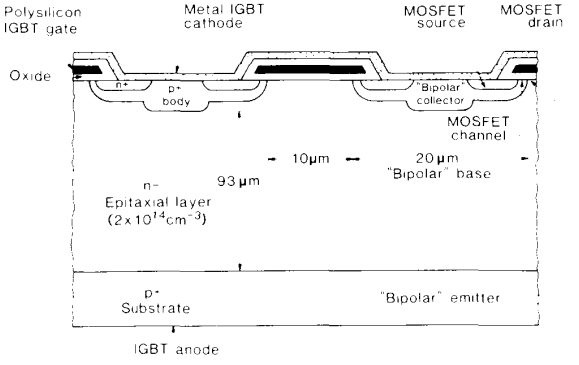

Fig.1. A diagram of two of the many thousand diffused cells of an n-channel IGBT.

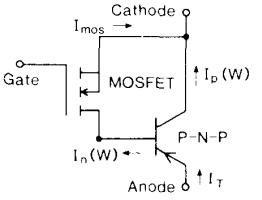

Fig.2. The equivalent circuit model of the IGBT.

II. ANALYTICAL IGBT MODEL

In this section, the previously developed analytical model which describes the steady-state and transient operation of the IGBT is presented [4,5]. This model is based on the equivalent circuit of Fig. 2. The model was derived using ambipolar transport to describe the transport of electrons and holes in the low-doped epitaxial layer. The model differs substantially from the quasi-static approach for transient conditions. The description given in this paper is for an n-channel device.

A. IGBT DEVICE PHYSICS

Because of the IGBT structure, the bipolar transistor base current (electrons) supplied by the MOSFET is introduced at the collector end of the base. In the model, the region of the device at the epitaxial layer edge of the reverse-biased epitaxial layer-body junction, where the excess carrier concentration is zero, is designated as the contact between the bipolar transistor base and the MOSFET drain. The electron current that enters this region is equal to the MOSFET current, and the hole

* Contribution of the National Bureau of Standards; not subject to copyright.

88CH2565-0/88/0000-0606$01.00 © 1988 IEEE

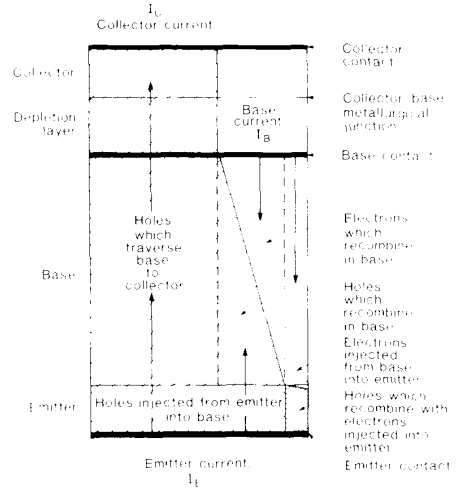

Fig.3. A schematic of the flow of carriers in the bipolar transistor of the IGBT indicating the position of the base virtual contact.

current there is the collector current of the bipolar transistor. A schematic of the flow of carriers in the base of the bipolar transistor of the IGBT is shown in Fig. 3.

Because the base of the bipolar transistor of the IGBT is in the high-level injection condition for the practical current density range of the device, $n \approx p$ and the transport of electrons and holes in the base are described by the ambipolar transport equations [8]

$$I_n = \frac{b}{1+b} I_T + qAD \frac{\partial p}{\partial x} \tag{1}$$

$$I_p = \frac{1}{1+b} I_T - qAD \frac{\partial p}{\partial x}, \tag{2}$$

where the symbols are defined in the Nomenclature. Notice that both of these expressions depend on the total current so that the transports of electrons and holes are coupled by I_T and cannot be treated independently. The time-dependent ambipolar diffusion equation is given by

$$\frac{\partial^2 \delta p}{\partial x^2} = \frac{\delta p}{L^2} + \frac{1}{D} \frac{\partial \delta p}{\partial t}. \tag{3}$$

This equation is valid only for devices in which I_T is independent of position, which is satisfied for the bipolar transistor of the IGBT because the base contact is at the collector end of the base.

B. STEADY-STATE

In this subsection, a system of parametric equations is presented for the steady-state collector and base currents, the excess carrier concentration, and the emitter-base voltage of the bipolar transistor of the IGBT. The bipolar transistor equations are then combined with a simple model for the MOSFET portion of the device to describe the on-state current voltage characteristics of the IGBT. The bipolar transistor analysis is performed using the coordinate system defined in Fig. 4.

1) Excess Carrier Concentration: The collector-base junction of the bipolar transistor of the IGBT is reverse biased for forward conduction and the collector-base junction depletion

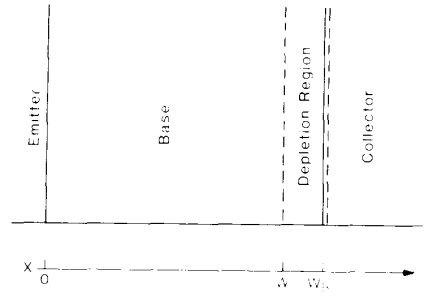

Fig.4. Coordinate system used in developing the IGBT model.

width is given by

$$W_{bcj} = \sqrt{\frac{2\epsilon_{si}(V_{bc} + V_{bi})}{qN_B}}, \tag{4a}$$

where $V_{bi} \approx 0.7\ V$. The width of the quasi-neutral base is then given by

$$W = W_B - W_{bcj}. \tag{4b}$$

The excess carrier concentration at $(x = W)$ is zero and the solution to the steady-state ambipolar diffusion equation ((3) with $\partial \delta p / \partial t = 0$) in the base is

$$\delta p(x) = P_0 \frac{\sinh(\frac{W-x}{L})}{\sinh(\frac{W}{L})}, \tag{5}$$

where the carrier concentration at the base edge of the emitter-base junction P_0 is used as a parameter for the development of the model. The total excess carrier charge in the base is found by integrating this carrier distribution through the base

$$Q = qP_0AL \tanh \frac{W}{2L}. \tag{6}$$

This parameter is used as an initial condition for the transient analysis.

2) Collector and Base Currents: Using the quasi-equilibrium approximation and assuming high-level injection in the base, the electron current injected into the emitter is given by

$$I_n(x = 0) = I_{sne} \frac{P_0^2}{n_i^2}, \tag{7}$$

where I_{sne} is the emitter electron saturation current and takes the emitter parameters into account. The base and collector currents are then obtained from (1), (2), (5) and (7):

$$I_B = \frac{P_0^2 I_{sne}}{n_i^2} + \frac{qP_0AD}{L}\left(\coth(\frac{W}{L}) - \frac{1}{\sinh(\frac{W}{L})}\right) \tag{8}$$

$$I_C = \frac{P_0^2 I_{sne}}{bn_i^2} + \frac{qP_0AD}{L}\left(\frac{\coth(\frac{W}{L})}{b} + \frac{1}{\sinh(\frac{W}{L})}\right), \tag{9}$$

where the base current is $I_n(x = W)$ and the collector current is $I_p(x = W)$ (see Figs. 2 and 3). The total IGBT anode current

is given by $I_T = I_B + I_C$ and is used as an initial condition for the transient analysis.

3) Anode Voltage: Because the base contact has been defined to be at the collector edge of the quasi-neutral base, the emitter-base voltage of the bipolar transistor includes the potential drop across the conductivity modulated base. The emitter-base voltage drop is given in terms of the parameter P_0 by [4-7]

$$V_{eb} = \frac{kT}{q}\ln\left(\frac{P_0^2}{n_i^2}\right) + \frac{I_T W}{(1+\frac{1}{b})\mu_n A q n_{eff}} - \frac{D}{\mu_n}\ln\frac{P_0+N_B}{N_B}, \quad (10)$$

where

$$n_{eff} \equiv \frac{\frac{W}{2L}\sqrt{N_B^2 + P_0^2\,\mathrm{csch}^2(\frac{W}{L})}}{\mathrm{arctnh}\left[\dfrac{\sqrt{N_B^2 + P_0^2\,\mathrm{csch}^2(\frac{W}{L})}\,\tanh(\frac{W}{2L})}{N_B + P_0\,\mathrm{csch}(\frac{W}{L})\tanh(\frac{W}{2L})}\right]}. \quad (11)$$

The first term on the right-hand side of (10) can be identified as the emitter-base junction high-level injection potential drop, the second term can be identified as the resistive drop across the conductivity modulated base where n_{eff} is the effective carrier concentration which depends on P_0, and the last term can be identified as the high-level injection diffusion potential due to the difference in carrier concentration across the base.

The on-state anode-cathode voltage drop of the IGBT is given by the sum of the emitter-base voltage and the collector-base voltage (Fig. 2),

$$V_A = V_{eb} + V_{bc}, \quad (12)$$

where the small series resistance due to bonding wires [4-6] is neglected in this paper for simplicity. It can be seen from Fig. 2, that $I_{mos} = I_B$ and that the collector-base voltage is equal to the drain-source voltage of the MOSFET. Because the MOSFET is in its linear region when the IGBT is in the on-state,

$$V_{bc} = \frac{I_B}{K_p(V_{gs} - V_T)}, \quad (13)$$

where the parameter K_p is equal to the product of the oxide capacitance, the surface electron mobility, and the effective width-to-length ratio of the MOSFET cells. The anode voltage is given in terms of P_0 using (8) through (13), which is obtained in terms of I_T from (8) and (9). Therefore, the IGBT on-state anode-cathode voltage drop is given explicitly in terms of anode current and gate voltage, assuming $V_{bc} \approx 0$ in (4). V_A is used as an initial condition for the transient analysis.

C. SWITCHING TRANSIENT

In this subsection, an analytical model is presented which describes the switching transient behavior of the IGBT. The basic model consists of two state equations which describe the state of the anode voltage V_A' and the charge Q' of the IGBT. These equations are integrated simultaneously with the state equations of the load circuit using the initial conditions from the steady-state device analysis to obtain the current and voltage versus time. Parameters that change with time are distinguished with a prime for the transient analysis.

To turn off the IGBT, the gate voltage is switched below threshold, which rapidly removes the MOSFET channel current and eliminates the base current to the bipolar transistor. The bipolar transistor collector current falls more slowly though, since the stored excess carriers in the now open-base bipolar transistor must decay. For simplicity, the effects of the driving circuit are not considered in this work, but the analysis presented in this paper can be extended to include the driving circuit [9]. The simulations and measurements of this work are made for rapid gate voltage transitions so the MOSFET portion of the device is turned off rapidly and the bipolar base current is zero during the transient.

Because the boundary conditions on the electron and hole currents are different between the steady-state and the transient conditions, the shape of the excess carrier distribution and the relationship between the current and the total excess carrier charge in the base are different during the transient than during steady-state. This means that the commonly used quasi-static approximation is not valid for the IGBT. The quasi-static approximation assumes that the relationship between the total base charge and the current is the same during the transient as it is for similar steady-state conditions [10]. The difference exists for two reasons: 1) the electron and hole transport equations are coupled for ambipolar transport so the collected hole current is changed with the removal of the MOSFET electron current which is large for the IGBT because of the low current gain, and 2) during anode voltage transitions, the collector-base depletion width is changing faster than the base-transit time for excess carriers so a significant component of current is required to redistribute the carriers into the changing base width.

1) Excess Carrier Concentration: During anode voltage transitions, the collector-base depletion width changes with time and is given in terms of the collector-base voltage by (4a). Thus, the quasi-neutral base width, given by (4b), also changes with time. Because the base width changes with changing voltage, the excess carrier charge Q' is swept into a narrower neutral base as the voltage is increased. This is illustrated in Fig. 5 where the change in the local excess carrier concentration Δp due to the change in the base width ΔW is indicated. A divergence in the electron and hole currents and a corresponding curvature in the carrier distribution is required to bring about this changing local carrier concentration.

A first-order solution to (3) for the conditions of a moving collector-base depletion edge is given by [4,5]

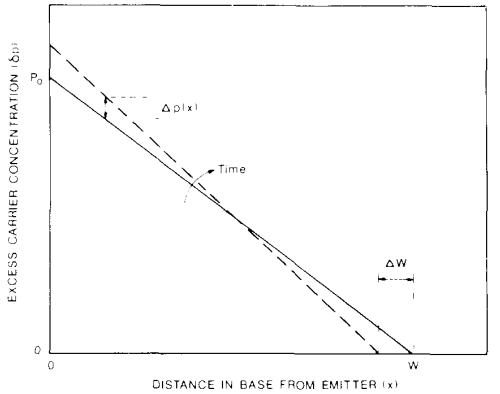

Fig.5. The carrier distribution in the base indicating the change in excess carrier concentration with time due to the moving collector-base depletion edge boundary.

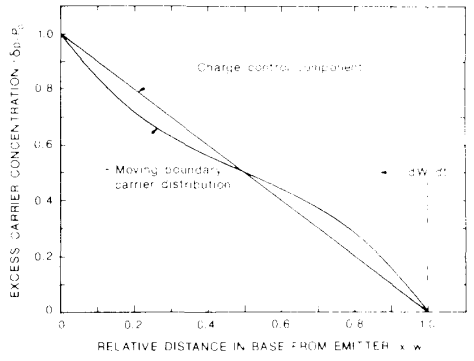

Fig.6. The excess carrier distribution in the base under the conditions of a moving collector-base depletion edge boundary.

$$\delta p'(x) = P_0'\left[1 - \frac{x}{W'}\right] - \frac{P_0'}{W'D}\left[\frac{x^2}{2} - \frac{W'x}{6} - \frac{x^3}{3W'}\right]\cdot\frac{dW'}{dt}, \quad (14)$$

where the collector-base depletion edge velocity dW'/dt is due to the expanding collector-base depletion region during voltage transitions according to (4). This carrier distribution is shown in Fig. 6 and has the curvature necessary to change the carrier distribution as indicated in Fig. 5 for a given collector-base depletion edge velocity. For a constant anode voltage, only the first term on the right-hand side of (14) remains. This term differs from the steady-state carrier distribution because the electrons and holes that recombine in the base are no longer supplied by the divergence of their current densities as they are in steady-state, but are only supplied by (and thus reduce) the local excess carrier concentration.

During the transient, the excess carrier base charge decays by recombination in the base and by electron injection into the emitter,

$$\frac{dQ'}{dt} = -\frac{Q'}{\tau_{HL}} - I_n'(x=0). \quad (15)$$

By integrating (14) through the base, the carrier concentration at the emitter edge of the base for the transient condition is given in terms of the total base charge by $P_0' = 2Q'/(qAW')$. Using (7) and (15), the rate of decay of the total excess base charge due to recombination and injection into the emitter is given by

$$\frac{dQ'}{dt} = -\frac{Q'}{\tau_{HL}} - \frac{4Q'^2 I_{snc}}{W'^2 A^2 q^2 n_i^2}, \quad (16)$$

where W' is given in terms of voltage by (4).

2) Electron and Hole Currents: For the case in which the MOSFET current is zero during the transient, the electron current at the collector edge of the quasi-neutral base is equal to the displacement current of the collector-base junction depletion capacitance. Equating the displacement current to (1) evaluated at $x = W'$ gives

$$C_{bcj}'\frac{dV_{bc}'}{dt} = \frac{b}{1+b}I_T' + qAD\frac{\partial p'}{\partial x}\Big|_{x=W'}. \quad (17)$$

The last term on the right-hand side of (17) is due to the collected hole current and is evaluated using the carrier distribution of (14):

$$-qAD\frac{\partial p'}{\partial x}\Big|_{x=W'} = \frac{2D}{W'^2}Q' - \frac{Q'}{3W'}\cdot\frac{dW'}{dt}. \quad (18)$$

The first term on the right-hand side of this expression is a charge control term because this component of current is directly related to the charge that remains in the base and to the applied collector-base voltage (using (4)). The second term on the right-hand side of this expression is the moving boundary redistribution component of current which depends on the rate of change of the collector-base depletion width as well as the charge and applied collector-base voltage.

3) Anode Voltage: The collector-base voltage is given in terms of anode voltage by (12), where the emitter-base voltage is held constant at its steady-state value for the transient analysis because the anode voltage is much larger than the emitter-base voltage during the transient. Therefore, $dV_{bc}'/dt = dV_A'/dt$ and the rate of change of the base width is given in terms of the rate of change of anode voltage using (4). The voltage rate of rise is then obtained from (17) and (18),

$$\frac{dV_A'}{dt} = \frac{I_T' - \frac{4D_p}{W'^2}Q'}{C_{bcj}'\left(1+\frac{1}{b}\right)\left[1+\frac{Q'}{3qAN_BW'}\right]}, \quad (19)$$

in terms of the current I_T', charge Q', and voltage V_A' (using (4) and (12)). The last term in the brackets in the denominator is a result of the moving boundary redistribution effect on the collected current and is equal to one-third times the ratio of the total excess carrier charge Q' to the background mobile carrier charge of the undepleted base (qAN_BW'). This term appears as a multiplicative factor because the redistribution current is proportional to dV_A'/dt just as is the displacement current. Because most of the base is in the high-level injection condition, this term is large compared to 1 and the redistribution current has a dominant effect on the voltage rate of rise.

For large voltages, the effect of mobile carriers in the depletion region has a significant effect on W'. The space charge concentration in the depletion region is given by

$$N_B' = N_B + \frac{I_p'(x=W')}{qAv_{psat}}. \quad (20)$$

This effect is accounted for by calculating the space charge concentration given by (20) at each evaluation of (19) using an iterative procedure.

III. LOAD CIRCUIT STATE EQUATIONS

The state variables required to describe the IGBT during the transient operation are V_A' and Q'. The state equations of the IGBT are given by (16) and (19), which are functions of the excess carrier base charge Q', the anode voltage V_A', and the anode current I_T'. The current I_T' is determined by the state equations of the load circuit where, in general, the load circuit contributes a state equation for each reactive element in the load. The switching current and voltage waveforms are then obtained for a given circuit by simultaneously integrating the state equations of the IGBT ((16) and (19)) with those for the load circuit using the initial values of the current, voltage, and charge from the steady-state device analysis. The simultaneous integration of the state variables is performed using a readily available subroutine called RKF45 (an automatic Runge-Kutta-Fehlberg method) [11].

As an example, the state equation contributed by the series

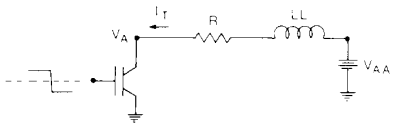

Fig.7. Circuit configuration of a series resistor-inductor load switching transient.

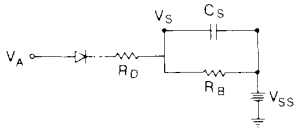

Fig.8. Protection circuit which is connected to the IGBT anode for the series resistor-inductor load of Fig. 7.

resistor-inductor load circuit shown in Fig. 7 is

$$\frac{dI'_L}{dt} = \frac{1}{LL}(V_{AA} - R\,I'_L - V'_A) \tag{21}$$

where $I'_T = I'_L$. In this case, the state variables are I'_L, V'_A, and Q'. Equations (16), (19), and (21) can also be reduced to describe clamped infinite inductive load switching or constant anode supply voltage switching, which results in a reduction of the number of state variables. To include the protection circuit shown in Fig. 8, the state equation

$$\frac{dV'_S}{dt} = \begin{cases} \dfrac{V'_A - V'_S - V_{bi}}{C_S R_D} - \dfrac{V'_S - V_{SS}}{R_B C_S} & \text{for} \quad V'_A > V'_S + V_{bi} \\ -\dfrac{V'_S - V_{SS}}{R_B C_S} & \text{for} \quad V'_A < V'_S + V_{bi} \end{cases} \tag{22}$$

is added. The anode current for this loading condition is given in terms of the state variables I'_L, V'_A, and V'_S by

$$I'_T = \begin{cases} I'_L - \dfrac{V'_A - V'_S - V_{bi}}{R_D} & \text{for} \quad V'_A > V'_S + V_{bi} \\ I'_L & \text{for} \quad V'_A < V'_S + V_{bi} \end{cases} \tag{23}$$

Because the diode is modeled by a voltage offset V_{bi} and a small resistance R_D for the forward bias condition and by an open circuit for the reverse-bias conduction, the two cases require the two different expressions in both (22) and (23).

The bleeder resistor R_B is used to determine the initial condition of the snubber voltage at the time the turn-off transient is initiated. If the bleeder resistor is connected to V_A instead of to the constant supply, the protection circuit is commonly referred to as a polarized turn-off snubber (or shunt snubber) [12,13]. In this case, the initial condition of V_S depends on the frequency and the duty cycle for a given R_B, but for long on-state times it approaches the IGBT on-state voltage. If the snubber supply voltage is connected as shown in Fig. 8, the protection circuit reduces to a voltage clamping circuit [14]. For this configuration, the initial condition of V_S depends on the frequency for a given bleeder resistor, but it approaches V_{SS} for single pulses (low frequencies) and $V_{SS} \geq V_{AA}$. For a repetitive waveform, the initial condition is obtained by iterating the solution until $V_S(t+T) = V_S(t)$ where T is the period of the repetitive waveform.

IV. SIMULATED AND MEASURED RESULTS

In this section, measurements of the switching transient characteristics of the IGBT for several loading conditions are compared with the simulations. Simplified loading conditions are first used to independently verify both of the device state equations ((16) and (19)). Equations (16), (19), and (21) are then used to simulate the current and voltage waveforms of the IGBT for the series resistor-inductor load and to determine the conditions for which the IGBT can be switched safely. Finally, for those conditions in which the IGBT cannot be switched safely with the series resistor-inductor load, (16), (19), and (21) through (23) are used to simulate the current and voltage waveforms of the series resistor-inductor load including the protection circuit of Fig. 8. The experimental verification and device simulations are performed for devices with different values of base lifetime and the physical parameters listed in Table I except that $W_B = 110\ \mu m$ is used for the 0.3-μs device.

TABLE I
DEVICE MODEL PARAMETERS

n_i	$1.45 \times 10^{10}\ cm^{-3}$
μ_n	$1500\ cm^2/Vs$
μ_p	$450\ cm^2/Vs$
ϵ_{si}	$1.05 \times 10^{-12}\ F/cm$
v_{psat}	$10^7\ cm/s$
N_B	$2 \times 10^{14}\ cm^{-3}$
A	$0.1\ cm^2$
W_B	$93\ \mu m$
I_{sne}	$6.0 \times 10^{-14}\ A$
K_p	$0.36\ A/V^2$

A. DEVICE MODEL VERIFICATION

Verification of the steady-state IGBT model has been presented elsewhere [4-6] and will not be repeated here. To verify the IGBT transient model, both constant voltage and constant current conditions are examined and results are compared for different voltages, currents, and device lifetimes. In doing this, both (16) and (19) are independently verified. The constant current condition is obtained by using a clamped inductive load with a large ($\sim 1\ mH$) inductance. Before the clamp voltage is reached, the large inductance requires the anode current to remain constant at the initial value determined by the steady-state conditions. The constant anode voltage condition is obtained for two different load circuits: 1) for clamped inductive load switching with a large clamp capacitor, the voltage remains constant after the clamp voltage is reached, and 2) for constant anode supply voltage switching ($R = 0$ and $L = 0$), the anode voltage is held constant with a large-valued, low-inductance capacitor connected to the anode and the current is determined by varying the steady-state gate voltage.

First consider the current waveform for constant anode supply voltage switching which is shown in Fig. 9. The current waveform consists of an initial rapid fall due to (but not equal to) the removal of the MOSFET current, followed by a slowly decaying phase due to remaining slowly decaying excess carriers in the base. After the MOSFET portion of the current is removed, the current waveform is described by (16) and (19). For the constant voltage condition, (19) reduces to an algebraic equation for the current in terms of charge

$$I'_T = \frac{4D_p}{W'^2}Q', \tag{24}$$

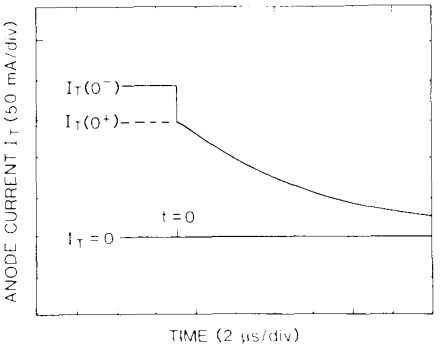

Fig.9. Data from an oscillogram of a 10-V constant anode voltage turn-off current waveform, noting the current before and after the initial rapid fall, $I_T(0^-)$ and $I_T(0^+)$, respectively.

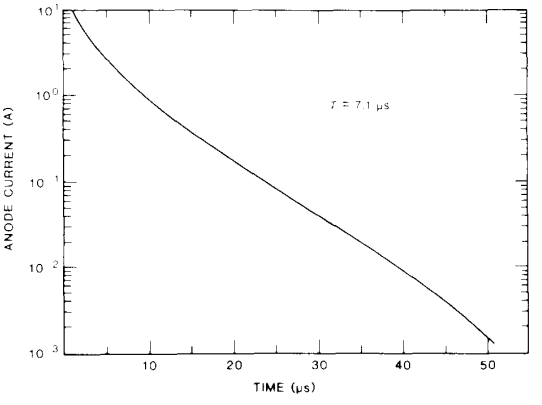

Fig.10. The charge control current decay path obtained by superimposing nine (9), one-decade-long, digitized current decay waveforms taken at different initial currents.

where W' is constant for constant anode voltages which are much larger than the emitter-base voltage, neglecting the effect of mobile carriers on the depletion region space charge concentration. The current versus time is then obtained by integrating (16). Because the current is equal to a constant times the charge, (16) indicates that the current decays exponentially with a time constant of τ_{HL} at low currents and that at high currents the rate is increased due to injection of electrons into the emitter.

Figure 10 shows the measured slowly decaying portion of the current decay waveform over several decades on a semi-log scale. Notice that the current decay rate is nearly constant in the intermediate current range and that it increases at both low and high currents. The decay rate increases at low currents (below 20 mA) because the base leaves the high-level injection condition and the low-level lifetime is smaller than the high-level lifetime. All subsequent measured and simulated results are for currents above 20 mA where the assumption of high-level injection is valid. This is a practical current range for the IGBTs studied in this work. The increased decay rate at high currents is due to injection of electrons into the emitter as discussed in the last paragraph. In the intermediate current range, the base is in high-level injection and the injection of electrons into the emitter is negligible. Therefore, the decay rate in the intermediate current range is used to extract the high-level base lifetimes [4-6].

Next, consider the clamped inductive load with a large inductor ($\sim 1\ mH$) and a large clamp capacitor. Before the clamp voltage is reached, the large inductance requires the anode current to remain constant at the initial value determined by the

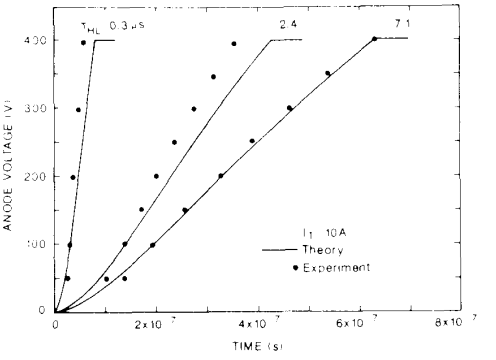

Fig.11. A comparison of the theoretical and measured 10-A infinite inductive load turn-off voltage waveforms for devices with different base lifetimes.

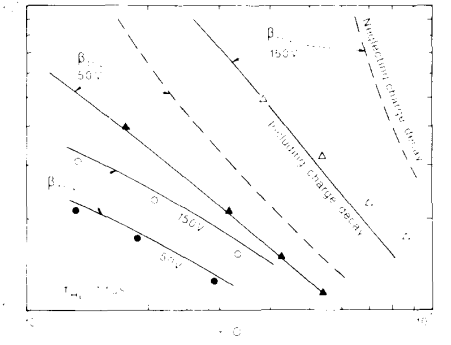

Fig.12. A comparison of the theoretical (solid curves) and measured (● ○ ▲△) values of β_{tr} versus current for both constant anode supply voltage switching and clamped inductive load switching at 50 V and 150 V for a 7.1-μs device. The dashed curves are the calculated values of $\beta_{tr,L}$ neglecting the decay of charge during the voltage transition.

steady-state conditions. Measured and simulated large inductor voltage waveforms are compared in Fig. 11 for devices with different base lifetimes at a current of 10 A. The simulated voltage waveforms were obtained by simultaneous integration of (16) and (19) with I_T' equal to the steady-state current. Notice that the voltage rate of rise varies significantly with device base lifetime. This is caused by the effective increase in the collector-base capacitance due to the moving boundary redistribution current. After the clamp voltage is reached, the anode voltage remains equal to the clamp voltage and the current decays similarly to that of the constant anode supply voltage switching shown in Fig. 9. The initial rapid fall in current is due to the removal of the moving boundary redistribution current and the collector-base junction depletion capacitance displacement current. Because the anode voltage is constant, the current decay is determined using (24) and (16) with the initial condition of the charge that remains at the time the clamp voltage is reached.

The ratio of the initial value of the slowly decaying portion of the current decay waveform to the magnitude of the initial rapid fall in current is defined as

$$\beta_{tr} = \frac{I_T'(0^+)}{I_T(0^-) - I_T'(0^+)}, \tag{25}$$

where $I_T(0^-)$ is the steady-state anode current given by the sum of (8) and (9), and $I_T'(0^+)$ is the initial value of the slowly

decaying portion (see Fig. 9). Figure 12 compares the measured and calculated values of β_{tr} for constant anode supply voltage switching ($\beta_{tr,V}$) and β_{tr} for large inductor load switching ($\beta_{tr,L}$) versus current both at two different voltages. The values of $\beta_{tr,L}$ differ from the values of $\beta_{tr,V}$ because the excess carrier base charge is swept into a narrower base (narrower than for steady-state) during the voltage rise and because some of the charge decays during the voltage rise. The dashed curves in Fig. 12 show the effects of neglecting this decay by using the steady-state charge in (24) to calculate $I_T'(0^+)$. The agreement between the model and the experiment for $\beta_{tr,V}$ indicates that the value of steady-state charge used by the model is adequate for an initial condition of the transient. The agreement between the theory and experiment for $\beta_{tr,L}$ at different voltages indicates that the charge decay is properly accounted for during anode voltage transitions. Therefore, both the charge and the voltage (see Fig. 11) state equations are verified.

B. DEVICE-CIRCUIT INTERACTIONS

Figure 13(a) shows the measured current and voltage switching waveforms for a series resistor-inductor load with $R = 31\ \Omega$, $LL = 5.5\ \mu H$, and $V_{AA} = 150\ V$. Figure 13(b) shows the simulated results for the same conditions as the measurements of Fig. 13(a). The simulations were made by simultaneously integrating (16), (19), and (21) with the initial conditions determined from the steady-state analysis. The theoretical and experimental waveforms are in good quantitative agreement with the exception that the ringing is damped more in the experiment. Notice in Figs. 13(a) and 13(b) that the voltage overshoots more and that the current approaches zero faster for the lower lifetime devices. The overshoot results from the stored energy in the inductor which is transferred to the effective device capacitance. It can be seen from Fig. 11 that the effective capacitance of the IGBT varies significantly with lifetime and that it is well described by the model.

The combinations of values of R, LL, V_{AA}, and τ_{HL} which are suitable for unprotected series resistor-inductor load switching with a fast gate voltage transition are limited. For example, Figs. 14 through 16 show the simulated and measured series resistor-inductor load current and voltage switching waveforms for values of inductance that can be safely switch. Each fig-

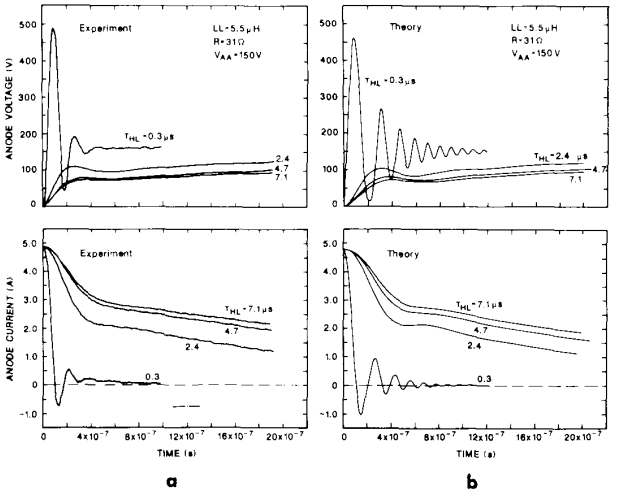

Fig.13. The measured (a) and simulated (b) series 31-Ω resistor, 5.5-μH inductor load current and voltage waveforms for devices with different lifetimes.

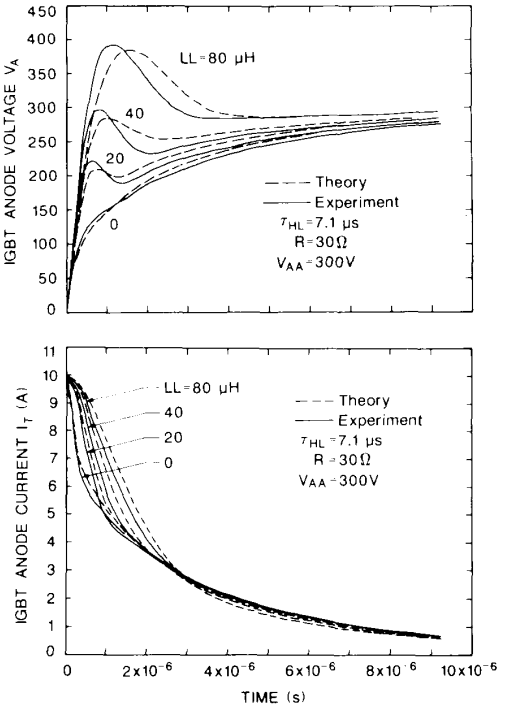

Fig.14. The measured and simulated series resistor-inductor load current and voltage waveforms for a 7.1-μs device and inductances from 0 to 80 μH.

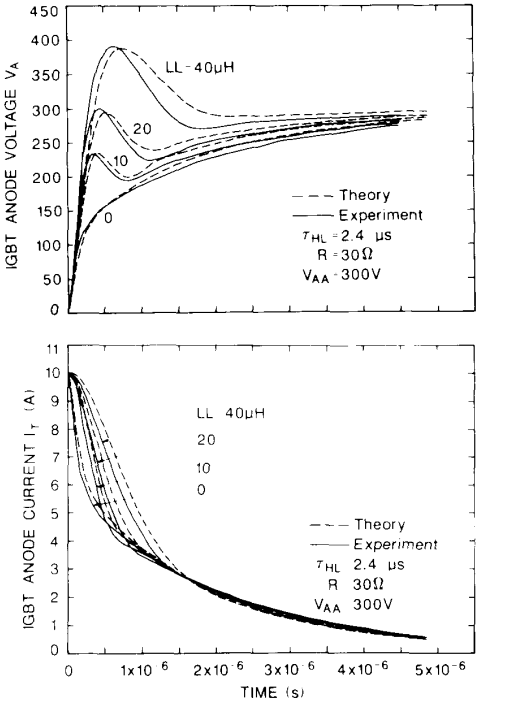

Fig.15. The measured and simulated series resistor-inductor load current and voltage waveforms for a 2.4-μs device and inductances from 0 to 40 μH.

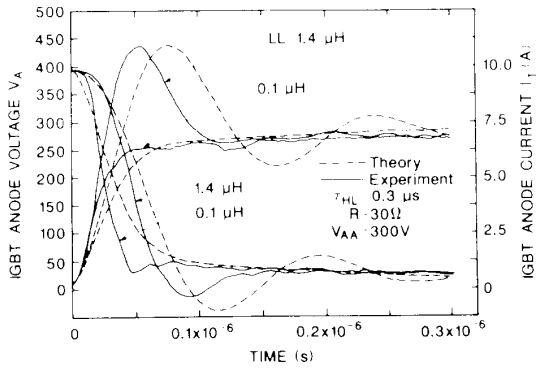

Fig.16. The measured and simulated series resistor-inductor load current and voltage waveforms for a 0.3-μs device and inductances of 0.1 to 1.4 μH.

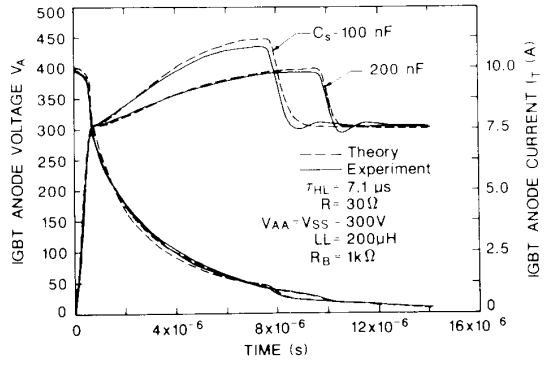

Fig.17. The simulated and measured snubbed series resistor-inductor load current and voltage waveforms for a 7.1-μs device, a 200-μH inductance, and two different snubber capacitances.

ure is for a different device lifetime. For inductances larger than 40 μH, the peak overshoot voltage for the 2.4-μs device (Fig. 15) approaches the BV_{CEO} of the IGBT (500 V) and the voltage will be clamped by the avalanche current. This is potentially destructive so a protection circuit must be added to the 2.4-μs device for load inductances larger than 40 μH. For otherwise identical conditions, the 7.1-μs device can switch 80 μH (Fig. 14) and the 0.3-μs device can switch 1 μH (Fig. 16) without exceeding 400 V. It has been shown that current snubbing can also increase the dynamic latch-up current of the IGBT [15,16].

The simulated and measured series resistor-inductor load current and voltage waveforms including the protection circuit of Fig. 8 are shown in Figs. 17 through 19 for inductances which are too large to be switched without a protection circuit. Each figure is for a different device lifetime and load inductance. Figures 17 and 18 include two different values of C_S. For lower values of C_S or larger LL, the overshoot will approach the device voltage rating. These figures demonstrate that the IGBT model can be used to determine the values of the protection circuit components needed for a given load circuit inductance. The simulations can also be used to examine other quantities of importance in the design of a snubber circuit, such as the switching energy of the device and the efficiency of the circuit.

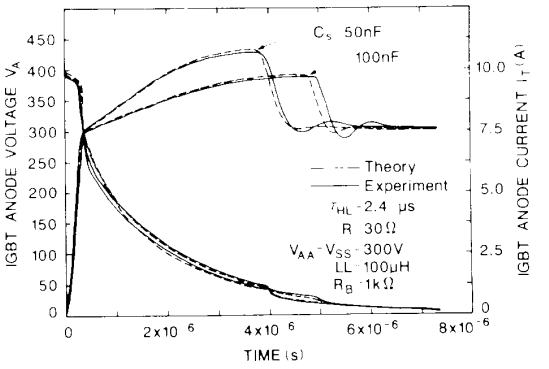

Fig.18. The simulated and measured snubbed series resistor-inductor load current and voltage waveforms for a 2.4-μs device, a 100-μH inductance, and two different snubber capacitances.

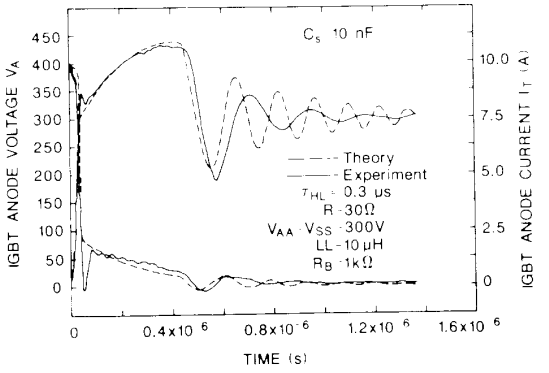

Fig.19. The simulated and measured snubbed series resistor-inductor load current and voltage waveforms for a 0.3-μs device and a 10-μH inductance.

V. CONCLUSION

A model has been developed for the IGBT which describes the steady-state condition and the switching transient current and voltage waveforms for general loading conditions. The interaction of the IGBT with the load circuit can be described using the device model and the state equations of the load circuit. The voltage rate of rise at turn-off for inductive loads varies significantly for IGBTs with different base lifetimes, and this rate of rise is important in determining the voltage overshoot for a given series resistor-inductor load circuit. Excessive voltage overshoot is potentially destructive, so a snubber protection circuit may be required. The protection circuit requirements are unique for the IGBT and can be examined using the model. Simulations of the device-circuit interactions have been experimentally verified for devices with different lifetimes.

ACKNOWLEDGMENT

The author would like to acknowledge D. L. Blackburn and D. W. Berning for their helpful discussions on the material of this paper. I would also like to thank E. J. Walters for preparing this manuscript for publication.

REFERENCES

[1] J. P. Russell, A. M. Goodman, L. A. Goodman, and J. M. Neilson, "The COMFET–A New High Conductance MOS-Gated Device," IEEE Electron Dev. Lett., vol. EDL-4, pp. 63-65, Mar. 1983.

[2] B. J. Baliga, M. S. Adler, R. P. Love, P. V. Gray, and N. D. Zommer, "The Insulated Gate Transistor: A New Three-Terminal MOS-Controlled Bipolar Power Device," IEEE Trans. Electron Dev., vol. ED-31, pp. 821-828, Jun. 1984.

[3] H. Yilmaz, W. R. Van Dell, K. Owyang, and M. F. Chang, "Insulated Gate Transistor Modeling and Optimization," in Tech. Dig. 1984 IEEE Intern. Elec. Dev. Meet., pp. 274-277.

[4] A. R. Hefner, "Characterization and Modeling of the Power Insulated Gate Bipolar Transistor," Ph. D. Dissertation, University of Maryland. Ann Arbor, MI: University Microfilms International, 1987.

[5] A. R. Hefner and D. L. Blackburn, "An Analytical Model for the Steady-State and Transient Characteristics of the Power Insulated Gate Bipolar Transistor," to be published in Solid-State Electronics.

[6] A. R. Hefner, D. L. Blackburn, and K. F. Galloway, "The Effect of Neutrons on the Characteristics of the Insulated Gate Bipolar Transistor (IGBT)," IEEE Trans. Nucl. Sci., vol. NS-33, pp. 1428-1435, Dec. 1986.

[7] A. R. Hefner and D. L. Blackburn, "Performance Trade-Off for the Insulated Gate Bipolar Transistor: Buffer Layer versus Base Lifetime Reduction," IEEE Trans. Power Electronics, vol. PE-2, pp. 194-207, Jul. 1987; also in Conf. Rec. 1986 IEEE Power Elec. Spec. Conf., pp. 27-38.

[8] W. van Roosbroeck, "The Transport of Added Current Carriers in a Homogeneous Semiconductor," Physical Review, vol. 91, pp. 282-289, Jul. 1953.

[9] E. Stein and D. Schroder, "Computer Aided Design of Circuits for Power Controlling with the New Power Elements MOSFET and SIT," in Conf. Rec. 1984 IEEE Ind. Appl. Soc. Meet., pp. 766-771.

[10] R. S. Muller and T. I. Kamins, Device Electronics for Integrated Circuits, pp. 266. New York, NY: Wiley, 1977.

[11] G. E. Forsythe, M. A. Malcolm, and C. B. Moler, Computer Methods for Mathematical Computations, pp. 129. New Jersey: Prentice-Hall, 1977.

[12] W. Mc Murray, "Selection of Snubbers and Clamps to Optimize the Design of Transistor Switching Converters," in Conf. Rec. 1979 IEEE Power Elec. Spec. Conf., pp. 62-74.

[13] A. Ferraro, "An Overview of Low-Loss Snubber Technology for Transistor Converters," in Conf. Rec. 1982 IEEE Power Elec. Spec. Conf., pp. 466-477.

[14] B. R. Nair and P. C. Sen, "Voltage Clamp Circuits for a Power MOSFET PWM Inverter," in Conf. Rec. 1984 IEEE Ind. Appl. Soc. Meet., pp. 797-806.

[15] H. W. Becke, C. E. Harm, R. T. Lee, H. R. Ronan, Jr. , and C. F. Wheatley, Jr. , "Applications of COMFETs (IGT) to 40 kHz Off-Line Switcher," in Conf. Proc. 1986 IEEE Appl. Power Elec. Conf., pp. 1-7.

[16] V. SuKumar and D. Y. Chen, "IGT/COMFET Latching Characteristics and Application to Brushless DC Motor Drive," IEEE Trans. Aerospace Elec. Syst., vol. AES-22, pp. 530-535, 1986.

NOMENCLATURE †

A	Device active area (cm^2).
I_n, I_p	Electron, hole current (A).
I_B, I_C	Base, collector current (A).
$I_T = I_B + I_C$	Anode current (A).
I_{mos}	MOSFET channel current (A).
I_L	Inductor current (A).
I_{snc}	Emitter electron saturation current (A).
n, p	Electron, hole carrier concentration (cm^{-3}).
δp	Excess carrier concentration (cm^{-3}).
P_0	δp at $x = 0$ (cm^{-3}).
n_i	Intrinsic carrier concentration (cm^{-3}).
n_{eff}	Effective base carrier concentration (cm^{-3}).
Q	Total excess carrier base charge (C).
ϵ_{si}	Dielectric constant of silicon (F/cm).
q	Electronic charge ($1.6 \times 10^{-19} C$).
μ_n, μ_p	Electron, hole mobility (cm^2/Vs).
D_n, D_p	Electron, hole diffusivity (cm^2/s).
τ_{HL}	Base high-level lifetime (s).
$b = \frac{\mu_n}{\mu_p}$	Ambipolar mobility ratio.
$D = 2\frac{D_n D_p}{D_n + D_p}$	Ambipolar diffusivity (cm^2/s).
$L = \sqrt{D\tau_{HL}}$	Ambipolar diffusion length (cm).
x	Distance in base from emitter (cm).
W_B	Metallurgical base width (cm).
W	Quasi-neutral base width (cm).
W_{bcj}	Collector-base depletion width (cm).
$C_{bcj} = \frac{A\epsilon_{si}}{W_{bcj}}$	Collector-base depletion capacitance (F).
N_B	Base doping concentration (cm^{-3}).
K_p	MOSFET channel transconductance (A/V^2).
V_{gs}	Gate-source voltage (V).
V_T	MOSFET channel threshold voltage (V).
V_{bi}	Built-in junction potential (V).
V_{bc}	Applied collector-base voltage (V).
V_{eb}	Applied emitter-base voltage (V).
V_A	Device anode voltage (V).
V_{AA}	Anode supply voltage (V).
V_S	Snubber voltage (V).
V_{SS}	Snubber supply voltage (V).
C_S	Snubber capacitance (F).
LL	Series load inductance (H).
R	Series load resistance (Ω).
R_B	Snubber bleeder resistance (Ω).
R_D	Diode resistance (Ω).

† Parameters that change with time are distinguished with a prime for the transient analysis.